

CrossMark  
click for updatesCite this: *J. Mater. Chem. B*, 2014, 2,  
6345

# Orange and blue luminescence emission to track functionalized porous silicon microparticles inside the cells of the human immune system†

N. Daldosso,<sup>a</sup> A. Ghafarinazari,<sup>a</sup> P. Cortelletti,<sup>b</sup> L. Marongiu,<sup>c</sup> M. Donini,<sup>c</sup> V. Paterlini,<sup>a</sup> P. Bettotti,<sup>b</sup> R. Guider,<sup>b</sup> E. Froner,<sup>b</sup> S. Dusi<sup>c</sup> and M. Scarpa<sup>\*b</sup>

Porous silicon micro-particles (micro-pSi) with size in the range of 1–10  $\mu\text{m}$  are obtained by etching of silicon wafers followed by sonication. The derivatization of the micro-pSi surface by wet chemistry (silylation and coupling with a diamine) yields an interface, which exposes negative (carboxylic) or positive (amine) groups at pH 7.4. The surface modification, beyond the introduction of groups for the drug loading by covalent or electrostatic interactions, stabilizes the intense orange luminescence characteristic of the silicon nano-crystallites. Derivatization by amines introduces also a second emission in the blue region, which follows a different excitation pathway and can be attributed to the interface defects. The micro-pSi are efficiently internalized by human dendritic cells and do not show any toxic effect even at a concentration of 1  $\text{mg mL}^{-1}$ . The intrinsic luminescence of the differently functionalized micro-pSi is preserved inside the cells and permits the selective and efficient tracking of the microparticles without using molecular tags and thus leaving the organic coating available for the interaction with the drug. The results obtained suggest that the functionalized micro-pSi are an efficient platform for simultaneous imaging and delivery of therapeutic agents to the disease site.

Received 25th June 2014  
Accepted 20th July 2014

DOI: 10.1039/c4tb01031k

[www.rsc.org/MaterialsB](http://www.rsc.org/MaterialsB)

## 1 Introduction

The use of micro-to-nanosized fragments of porous silicon (pSi) as a vehicle for delivery and controlled release of drugs or nanoparticles<sup>1–5</sup> is a promising strategy. In fact, the pSi morphology offers a large loading capacity and pSi in biological environments undergo dissolution, producing non-toxic and harmlessly removed wastes.<sup>6,7</sup> pSi show also an intrinsic visible photoluminescence (PL) that is derived from the combination of quantum confinement<sup>8,9</sup> and surface effects.<sup>10</sup> The intrinsic PL of pSi could allow the monitoring of the kinetics of the

carrier distribution and the localization of the delivery site of the loaded molecules in cell cultures and *in vivo*, without the need for a molecular tag such as fluorophores. Recently, Sailor *et al.*<sup>11</sup> reported about the use of oxidized and luminescent pSi particles in cells and in living animals; however, the PL of pSi-based drug delivery vehicles has been scarcely exploited so far. The reason is probably due to the loss of PL during the vehicle fabrication. In fact, the PL emission of pSi depends not only on the nanocrystallite size<sup>12</sup> but also on surface states.<sup>13</sup> Morphological properties<sup>14</sup> determine also the performances of pSi as a drug delivery vehicle and must be optimized to carry the load and reach the delivery site. The pore size, porosity and even the fragment size and shape can be changed by adjusting the fabrication protocols.<sup>15</sup> The pSi particles with dimensions spanning from micrometers to few hundreds of nanometers have been recently obtained<sup>16,17</sup> and different surface derivatization strategies have been suggested.<sup>18</sup> However, many chemical procedures require high temperatures<sup>16</sup> or exposition to nitrogen containing compounds,<sup>19</sup> which irreversibly quench the PL.<sup>20</sup> Stabilization of the PL of nanostructured silicon is obtained by mild surface oxidation,<sup>21</sup> however the surface coating by organic molecules is desirable since it improves the drug delivery properties. In particular, though the grafting of amino groups (that bear positive charge and have good coupling properties) is attractive,<sup>22</sup> it must be taken into account that amines are quenchers of the PL of pSi.<sup>20,23,24</sup> The control of surface chemistry is also important from the perspective of safe

<sup>a</sup>Department of Computer Science, Fluorescence Laboratory, University of Verona, Strada le Grazie 15, 37134 Verona, Italy. E-mail: nicola.daldosso@univr.it

<sup>b</sup>Department of Physics, Laboratory of Nanoscience, University of Trento, Via Sommarive 13, 38123 Trento, Italy. E-mail: marina.scarpa@unitn.it

<sup>c</sup>Department of Pathology and Diagnostics, Division of General Pathology, University of Verona, Strada le Grazie 8, 37134 Verona, Italy. E-mail: stefano.dusi@univr.it

† Electronic supplementary information (ESI) available: Fig. S1 shows the histogram of the size distribution of the porous silicon microparticles. Fig. S2 shows the FTIR spectrum of native porous silicon microparticles. Fig. S3 shows the FTIR spectra of porous silicon microparticles after surface derivatization. Fig. S4 shows the time course of the PL decay of the amine-micro-pSi (9  $\mu\text{g mL}^{-1}$ ) in aqueous solution. Fig. S5: panel (a) shows the decay of the PL of the functionalized micro-pSi in ethanol (emission 600 nm); panel (b) shows the lifetimes ( $\tau$ ) and  $\beta$  values obtained by fitting the stretched exponential function to the experimental PL decay of the amino-micro-pSi. Fig. S6 shows the decay of the PL of the functionalized micro-pSi in ethanol (emission 420 nm). See DOI: 10.1039/c4tb01031k

use of nanomaterials.<sup>25</sup> In this regard, a relevant limit for the medical use of inorganic nano- or micro-particles is their ability to stimulate the release of pro-inflammatory cytokines by immune cells, such as dendritic cells (DCs).<sup>26,27</sup> DCs possess a huge and diverse functional repertoire,<sup>28</sup> including the capacity of presenting the antigens to T lymphocytes in order to stimulate an immune response.<sup>29</sup> This last function makes DCs the preferential target of nanovaccines for cancer immunotherapy.<sup>30</sup>

In this study, we have optimized a fabrication and derivatization protocol, which permits the grafting of negative (carboxyl) or positive (amino) functionalities on micro-sized pSi particles (micro-pSi). This protocol preserves the intrinsic PL of pSi, though the grafting of the amino groups introduces different light emission pathways. We proved that the PL emission improves the tracking of the micro-pSi by using conventional optical instrumentation. The micro-pSi interaction with cells has been tested on human DCs. We found that the luminescent micro-pSi were efficiently internalized by DCs preserving their optical properties without inducing apoptosis, and without causing any pro-inflammatory response. These results suggest the safe use of these materials in biological environments and the efficient delivery of specific antigens to the immune system by micro-pSi.

## 2 Experimental

### 2.1 Materials

All the reagents and solvents used for the microparticle preparation and functionalization were purchased by Sigma-Aldrich (Milan) and were of the highest available purity. Hydrofluoric acid (HF 48%) was diluted in Teflon vessels and used under a fume cupboard conforming to the required standards.

### 2.2 Preparation of porous silicon microparticles

Porous silicon layers were formed by electrochemical etch of boron doped p-type Si wafers ((100) oriented, 10–20  $\Omega$  cm resistivity, University wafers, Boston MA). The etching was performed at constant current (80 mA cm<sup>-2</sup>) for 5 min in HF:ethanol. The porous layer was removed and fragmented into microparticles (micro-pSi) by 15 minutes sonication at 400 W in toluene (80 mL). The etching and sonication steps were repeated twice and about 30–35 mg of micro-pSi were produced. The residues of HF were removed by centrifugation at 500g (10 min) and the precipitate was re-suspended in 40 mL toluene. The native micro-pSi particles were stored in toluene under an argon atmosphere.

### 2.3 Surface modification of micro-pSi

An organic layer bearing carboxyl groups was introduced on the native micro-pSi surface by light-driven hydrosilylation.<sup>31</sup> The pristine micro-pSi were suspended in toluene saturated with argon and containing acrylic acid *N*-hydroxysuccinimide ester (5 mM). The solution was illuminated with white light (250 W) for two hours. Then the solution was centrifuged at 500g for 10 min. The powder (carboxyl-micro-pSi) was collected and

washed several times (at least 10 times) with ethanol or toluene. Ethanol was used to obtain free carboxylic groups on the powder surface. In fact, the reactive *N*-hydroxysuccinimide group (NHS) slowly hydrolyses in this solvent.<sup>32</sup> Conversely, the washing steps were performed in toluene if the powder underwent further modification by coupling with a diamine (see the next paragraph). If necessary, the powder suspended in ethanol was dried by centrifugation and the ethanol residues were removed by a gentle nitrogen flow. *N,N'*-Dicyclohexylcarbodiimide (final concentration 200  $\mu$ M) and 4,7,10-trioxo-1,13-tridecanediamine (200  $\mu$ M) were added to carboxyl-micro-pSi (30 mg) suspended in toluene (25 mL) and left to react for a night under gentle shaking. Then, the suspension was centrifuged and the powder (amine-micro-pSi) was purified from excess reagents and by-products by repeated washing with ethanol followed by centrifugation at 500g for 10 min. The carboxyl- and amine-micro-pSi were usually stored in ethanol or as dried powders.

### 2.4 Characterization of native micro-pSi, carboxyl-micro-pSi, and amine micro-pSi

Scanning Electron Microscopy (SEM) images were obtained by using a Zeiss SUPRA 40, with a thermal field emission source, operating at an accelerating voltage in a range of 1.5–5 kV. The analysis of the particle size distribution was done by optical microscopy using an Olympus microscope equipped with a 100 $\times$  magnification objective (MPlan, NA 0.9; Olympus) and 10 $\times$  oculars. Images were analysed using Fiji software.<sup>33</sup> The porosity was determined by gravimetric analysis<sup>34</sup> and the specific surface area was calculated according to Halimaoui.<sup>35</sup> The chemical groups present on the native or modified micro-pSi were investigated by Fourier Transform Infra-Red (FTIR) spectroscopy. The powder suspension was deposited on a ZnSe slab and left to dry under gentle nitrogen flow. The spectra were acquired by using a micro-FTIR Nicolet iN10 instrument, in the spectral range of 500–4000 cm<sup>-1</sup> with 4 cm<sup>-1</sup> resolution.

Steady-state fluorescence characterization and fluorescence life-times were performed by using a Horiba Jobin-Yvon Nanolog instrument. The configuration was: 2 nm slit size, 1200 g mm<sup>-1</sup> density grating (blazed 500 nm), 0.1 second integration time, and cut-off filtration at 370 nm. Lifetime analysis was carried out by the time-correlated single-photon counting method (TCSPC), with a xenon pulsed lamp as an excitation source. The obtained decays were fitted to a stretched exponential function having the general form:

$$I(t) = I_0 \exp[-(t/\tau)^\beta]$$

where  $I(t)$  is the PL intensity,  $\beta$  is the stretched parameter, and  $\tau$  is the lifetime. The lifetime of the amine-micro-pSi at 420 nm was measured with a pulsed nano-LED, characterized by an emission wavelength of 375 nm and a pulse duration of 1.2 ns. In this case, a single exponential function was used to fit the experimental decay curve. The PL of a single microparticle was obtained on an inverted Olympus Microscope iX70 by using a 488 nm solid state laser as an excitation source and an Avantes ULS2048XL-spectrometer.

## 2.5 Effect of micro-pSi on immune cell responses

After written informed consent and upon approval of the ethical committee, buffy coats from the venous blood of normal healthy volunteers were obtained from the Blood Transfusion Centre of the University of Verona. Monocytes were isolated from buffy coats by Ficoll-Hypaque and Percoll (GE Healthcare Life Science) density gradients and purified using the human monocyte isolation kit II (Miltenyi Biotec). The final monocyte population was 99% pure, as measured by FACS (Fluorescence-Activated Cell Sorting applied in flow cytometry) analysis. To generate dendritic cells (DCs), monocytes were incubated at 37 °C in CO<sub>2</sub> (5%) for 5–6 days at  $1 \times 10^6$  mL<sup>-1</sup> in 6-well tissue culture plates (Greiner, Nürtingen, Germany) in RPMI 1640, supplemented with heat-inactivated low endotoxin FBS (10%), L-glutamine (2 mM), GM-CSF (50 ng mL<sup>-1</sup>), and IL-4 (20 ng mL<sup>-1</sup>). The final DC population was 98% CD1a<sup>+</sup>, as measured by FACS analysis. The toxicity of the micro-pSi was tested using an Apoptosis Detection Kit (Miltenyi Biotec) according to the manufacturer's protocol. The percentages of live cells, dead cells and cells in the early apoptotic process were determined by Annexin V FITC conjugate and propidium iodide staining. Cells were acquired on a seven-colour MACSQuant Analyzer (Miltenyi Biotec) and FlowJo software (Tree Star, Ashland, OR, USA) was used for data analysis. Cytokine production in culture supernatants was determined using Ready-Set-Go ELISA kits purchased from Bioscience (San Diego, CA). The protein amount of IL-12 (range 4–500 pg mL<sup>-1</sup>), IL-23 (range 15–2000 pg mL<sup>-1</sup>), TNF- $\alpha$  (range 4–500 pg mL<sup>-1</sup>), IL-1 $\beta$  (range 4–500 pg mL<sup>-1</sup>) and IL-6 (range 2–200 pg mL<sup>-1</sup>) was analysed according to the manufacturer's protocol. For confocal microscopy analysis the DCs were seeded on 13 mm poly-L-lysine-coated cover slips and treated for 24 hours with the micro-pSi. The cells were washed with PBS and fixed with 4% paraformaldehyde (Sigma-Aldrich) for 30 min at room temperature and quenched with NH<sub>4</sub>Cl (50 mM). The cells were then permeabilized with PBS-Triton X-100 (0.1%) and blocked with BSA (1%) for 30 minutes. After washing, the cover slips were incubated for 30 minutes with Phalloidin-Rhodamine (Cytoskeleton, Denver, CO, USA) to visualize F-actin. The cells were washed and mounted in glycerol based anti-fading medium.

The images were acquired by using a confocal microscope (Leica-Microsystems, Wetzlar, Germany) at 400 $\times$  magnification by using the 63 $\times$  oil immersion objective (1.25 NA). Z-stacks were acquired and the maximum intensity projections (MIPs) were obtained by using the LAS-AF software (Leica-Microsystems).

## 3 Results and discussion

### 3.1 Characterization of micro-pSi

Fracture by sonication in anhydrous toluene of the pSi layer obtained by electrochemical etching produces a particle suspension, which emits in the region 590–620 nm under ultraviolet excitation. The SEM image shows that the particles are of irregular hemi-cylindrical shape (indeed there is uniformity among different particles) and the size of the major axis is

in the range 1–10  $\mu$ m (Fig. 1a) with a size distribution peaked at 1.5  $\mu$ m (see Fig. S1a, ESI<sup>†</sup>). The size of the minor axis is of the order of 100–300 nm (see Fig. S1b<sup>†</sup>). The lower size range (about 1  $\mu$ m) is determined under mild sonication conditions followed by a centrifugation step at 500g. In fact, we can estimate that the micro-pSi with size below the  $\mu$ m range do not sediment at 500g (ref. 36) and are discarded with the supernatant. The upper size range (about 10  $\mu$ m) is determined by the thickness of the pSi film. In fact, the mild sonication preferentially cleaves the pSi along the pores which are rather directional, propagating predominantly in the (100) crystallographic direction, perpendicular to the (100) face of the wafer.<sup>37</sup> The pores can be clearly visible as black spots in grey background of Fig. 1b, with an average diameter of about 30 nm. The average porosity determined by gravimetry on the porous silicon layer before sonication is 85%. This value corresponds to a specific surface area of 370 m<sup>2</sup> cm<sup>-3</sup>.<sup>35</sup> Native micro-pSi particles are hydride terminated and well dispersible in toluene.

Accordingly, the FTIR spectrum (Fig. S2, ESI<sup>†</sup>) shows the presence of Si-H<sub>3</sub> groups (at 2136 cm<sup>-1</sup>). However, oxidation is noticeable even after few minutes of air exposition, and the vibrational features of Si-O-Si (1038 cm<sup>-1</sup>) and OSiH<sub>x</sub> (2252 cm<sup>-1</sup>) are present in Fig. S2<sup>†</sup> together with the broad O-H band (at about 3300 cm<sup>-1</sup>). The micro-pSi suspension in toluene is stable and retains its PL for months if stored under anhydrous and anaerobic conditions. The surface of native Si nanocrystallites is vulnerable to attack by different compounds, such as amines which have been shown to quench the PL of free Si nanoparticles by opening non-radiative pathways to carrier relaxation.<sup>23</sup> We stabilized the PL of the native micro-pSi by suitable surface modification. In particular, we introduced on the pSi surface carboxyl groups (by hydrosilylation with NHS ester of acrylic acid) and amino groups (by a two-step procedure that is hydrosilylation with NHS ester of acrylic acid followed by diamine coupling). FTIR spectra (Fig. S3, ESI<sup>†</sup>) indicate that both reactions are successful; the characteristic vibrational bands of carboxyl ester signals (1735, 1788 and 1817 cm<sup>-1</sup>) appear after the reaction with acrylic acid-NHS. These peaks disappear after diamine coupling, while the amide I and II bands (1644 and 1550 cm<sup>-1</sup>) are observed and overlap a broad unresolved signal probably due to the bending of N-H. The presence of N-H groups is supported also by the features around 800 cm<sup>-1</sup> due to N-H wag. The two-step procedure does not determine quenching of PL due to the contact with the free diamine,<sup>23</sup> indicating that the micro-pSi surface was well protected by the acrylic-acid shell. The SEM images of the microparticles after functionalization with the diamine reveal an average decrease of the particle size and an enhancement in the surface roughness (Fig. 1c and d). Conversely, the average diameter of the pore is almost unaffected. The carboxyl or amine groups not only make the micro-pSi capable of interacting electrostatically with other molecules penetrating inside the pores but also can be used for the binding of a protective polymer shell to the external surface.

The amine-micro-pSi particles are well dispersed in polar solvents, but they agglomerate in toluene.

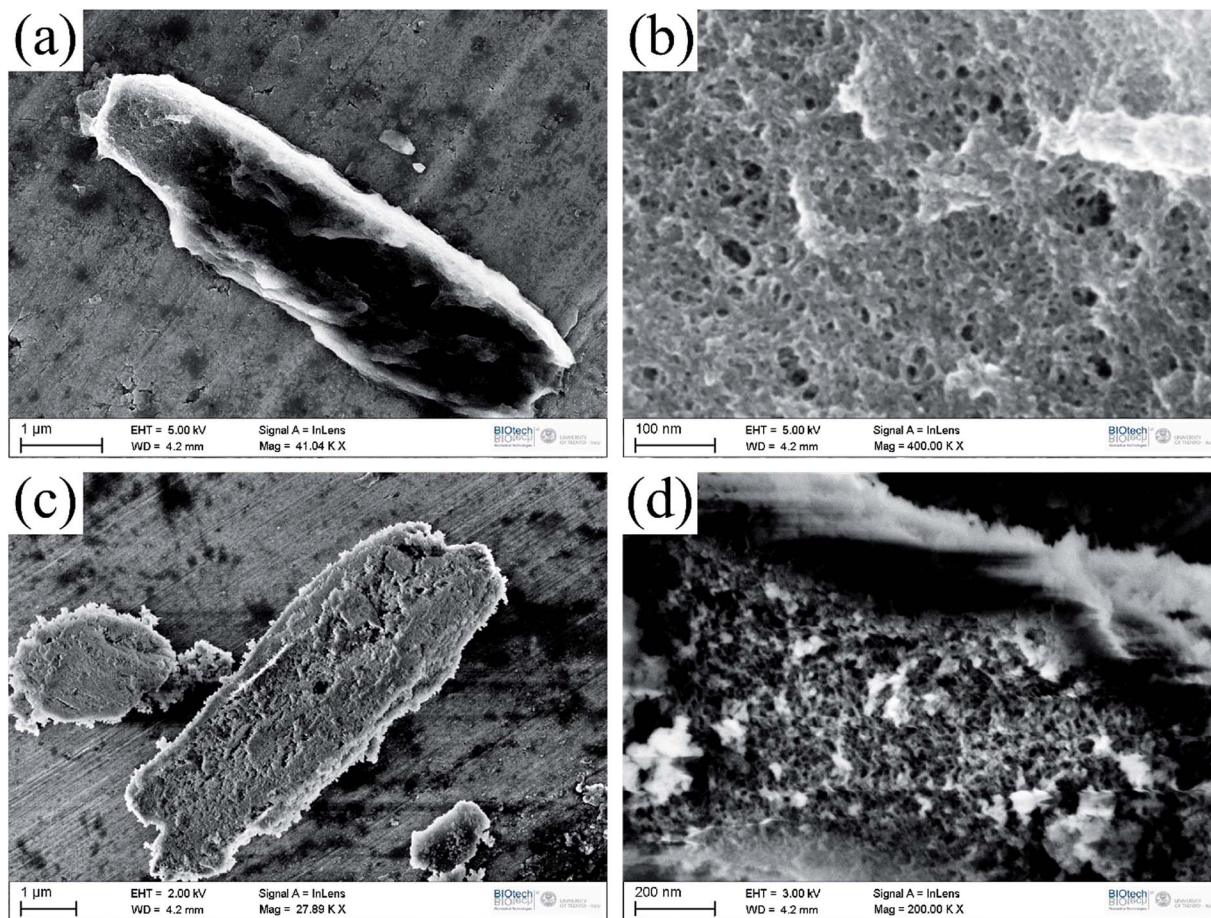


Fig. 1 SEM images of micro-pSi. A representative native micro-pSi just after sonication in anhydrous toluene (a) and a magnification of the porous structure (b). A representative micro-pSi carrying amino groups on the surface (c) and details of its surface roughness (d).

### 3.2 Optical properties of carboxyl- and amine-micro-pSi

The PL of the micro-pSi after the first and second functionalization steps (resulting in carboxyl- and amine-micro-pSi, respectively) was investigated and monitored over time. Fig. 2 reports the photoluminescence excitation (PLE) spectrum (detection wavelength 600 nm) of the carboxyl-micro-pSi (continuous trace) and the amine-micro-pSi (dashed trace). The PLE spectrum of carboxyl-micro-pSi is broader and centred at about 350 nm. The amine-micro-pSi PLE spectrum is shifted toward the blue region, probably because of partial oxidation induced by the amino groups.<sup>24</sup> PL emission of the carboxyl-micro-pSi and the amine-micro-pSi (continuous and dashed spectra, respectively) is reported in Fig. 3, left panel, for excitation at 350 nm. In both spectra, the typical broad emission characteristic of nanostructured silicon<sup>9,38</sup> with a maximum around 590–610 nm is present. This peak is blue shifted, and it is about 20 nm narrower in the case of the amine-micro-pSi. However, the PL spectrum of amine-micro-pSi displays another significant emission at 420 nm, which is neither typical of the Si nanocrystals obtained by pSi sonication<sup>39</sup> nor is observed in the spectrum of the carboxyl-micro-pSi. This band is characterized by a larger energy band-width with respect to that in the 590–610 nm range (the half-height band-width is 563 meV for the

emission at 420 nm and about 450 meV for that of the amino and carboxyl-micro-pSi at 590–610 nm). From the data of Fig. 2, where we showed also the PLE spectrum of the amine-micro-pSi

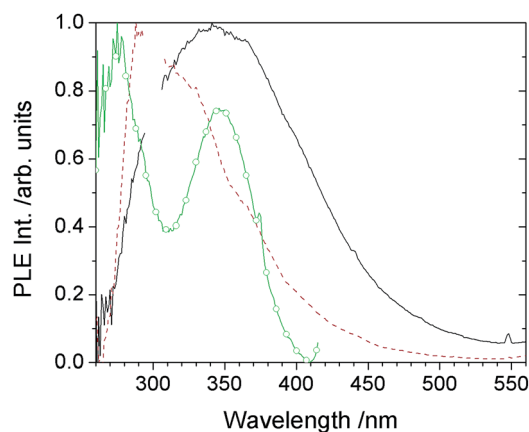


Fig. 2 Excitation spectra of functionalized micro-pSi. Solid trace: PLE of carboxyl-micro-pSi, the emission wavelength was 600 nm; dashed trace: PLE of amine-micro-pSi, the emission wavelength was 600 nm; dotted trace: PLE of amine-micro-pSi, the emission wavelength was 420 nm.

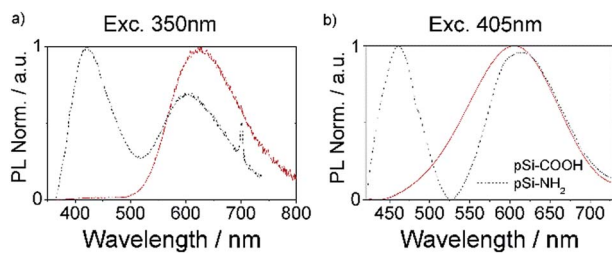


Fig. 3 Emission spectra of functionalized micro-pSi. The solid trace is for the carboxyl-micro-pSi and the dashed trace for the amine-micro-pSi. Left panel: excitation 350 nm. The sharp peak at 700 nm wavelength in the amine-micro-pSi sample is related to the second order of the spectrometer grating. Right panel: excitation 405 nm.

at a detection wavelength of 420 nm (dotted trace), it appears that the emission at 600 nm of the amine-micro-pSi (dashed trace) is excited with wavelengths in the 260–500 nm range, with a maximum at about 300 nm. Conversely, the emission at 420 nm (Fig. 2, dotted trace) has two main excitation peaks at about 275 and 350 nm. It appears also that both the carboxyl-micro-pSi and the amine-micro-pSi can be excited at 405 nm (which is the excitation wavelength used in confocal microscopy, see later on). The corresponding emission spectra are shown in Fig. 3, right panel, for the carboxyl-micro-pSi (continuous trace) and amine-micro-pSi (dashed trace). From this figure it appears that the emission in the blue region of the amine-micro-pSi by exciting at 405 nm is still intense and red-shifted, due to the proximity between excitation and emission wavelengths. The different peak feature and intensity of the PLE spectra acquired by looking at the two maximum emission peaks (as shown in Fig. 2) suggest that different mechanisms are responsible for the orange and the blue emission. The origin of the orange emission was attributed to quantum confinement effects in the silicon cores and to interfacial defects.<sup>40</sup> The blue one has been described for amine capped nanocrystals and attributed to the nitrogen impurities introduced at the silicon/silicon oxide interface.<sup>41</sup>

The PL degradation due to the ageing effect of the amine-micro-pSi in ethanol is very slow (we did not notice any detectable decrease after 8 months). Conversely, in water the PL half-life is about 3 days, as shown in Fig. S4 (ESI<sup>†</sup>), and is comparable to the half-life of the oxidized micro-pSi.<sup>21</sup> The PL decrease in water is clearly accompanied by the oxidation and dissolution of pSi. In fact, the emission band shifts toward shorter wavelength, in particular in the 600 nm region. To prove that dissolution occurs, we suspended the amine-micro-pSi (0.9 mg mL<sup>-1</sup>) in water (10 mL) for 10 days under gentle shaking and then centrifuged the sample. The amount of the collected precipitate (approximately 0.3 mg mL<sup>-1</sup>) was consistently decreased with respect to the starting suspended sample amount.

### 3.3 Lifetime measurements

The long emission lifetime (5–13  $\mu$ s) of micro-pSi is expected to open new perspectives to *in vivo* fluorescence imaging since

long-living emitters allow the elimination of tissue auto-fluorescence, which is a major obstacle confounding interpretation of *in vivo* fluorescence images. The functionalization process could affect the PL lifetime, since the radiative recombination rate is increased not only by quantum confinement but also by surface effects.<sup>41,42</sup> The time trace of the PL intensity of the carboxyl- and amine-micro pSi, shown in panel (a) of Fig. S5 in the ESI<sup>†</sup> (excitation at 350 nm and emission at 600 nm), was fitted by a stretched exponential function and a lifetime of about 18  $\mu$ s was found for both samples with a  $\beta$  value of 0.85. Since the major band of the PL spectrum of amino-micro-pSi is broad (the spectral peak spans over the range between 560 and 640 nm), we investigated the lifetime behaviour at different wavelengths. The experiment was performed by exciting at 350 nm the amine-micro-pSi suspended in ethanol, and the emission was monitored from 550 to 650 nm, taking an acquisition every 10 nm. The parameters  $\beta$  and  $\tau$  we obtained are reported in Fig. S5 panel (b) (ESI<sup>†</sup>). The long lifetimes together with their linear increase at increasing wavelength (the lifetime increases from 10 to 32  $\mu$ s in the interval 550–650 nm) suggest that the quantum confinement regime holds for the PL emission of the crystallites forming the porous matrix of the micro-pSi particles.<sup>40,42,43</sup>

The time trace of the blue band is shown in Fig. S6<sup>†</sup> (excitation at 375 nm and emission at 420 nm). A single exponential decay function was fitted to the experimental data and the resulting lifetime was found to be about 4 ns. This short lifetime is comparable with previous reports on blue emission from defects or impurity sites in silicon nanostructures upon exposure to nitrogen containing reagents.<sup>41,44</sup>

### 3.4 Effects on human dendritic cells

The cell uptake of micro-pSi was tested on human DCs since these cells mediate the immune response and are the preferential target of nanovaccines.<sup>30</sup> We performed experiments to analyse whether the micro-pSi affect human DC viability and/or cytokine release. The analysed cytokines include IL-12 that stimulates natural killer cells and T lymphocytes, as well as IL-23, which induces the secretion of pro-inflammatory mediators by T cells.<sup>45,46</sup> Moreover, we tested IL-6, IL-1 $\beta$ , and TNF- $\alpha$  which elicit the systemic acute phase reaction, characterized by fever, headache, anorexia, nausea, emesis, and changes in the sleep-wake cycle.<sup>27,47,48</sup> Human blood monocytes were cultured for 5 days with GM-CSF and IL-4 to obtain DCs, which were then challenged with various doses of micro-pSi or with lipopolysaccharide (LPS), a well-known bacterial immune cell stimulator, as a positive control. Fig. 4 shows the results of Annexin V staining experiments indicating that 24 hour exposure to different concentrations of carboxyl- and amine-micro-pSi did not induce DC apoptosis, even when a dose of 1 mg mL<sup>-1</sup> was added to the cells.

This finding is relevant considering that this dose is extremely high for the standard *in vitro* DC stimulation protocols. A 24 hour treatment of DCs with LPS did not affect cell viability (data not shown). We then analysed whether amine- or carboxyl-micro-pSi stimulate the release of pro-inflammatory

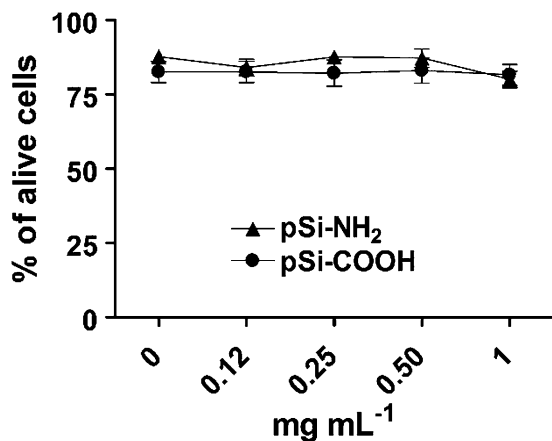


Fig. 4 Cell viability of human dendritic cells. DCs were treated with the indicated doses of carboxyl- and amine-micro-pSi for 24 hours. The incubation volume was 1 mL. The results are the mean  $\pm$  SD of three experiments.

cytokines by DCs. Fig. 5 illustrates an ELISA assay performed on DC culture supernatants showing that the amine-micro-pSi did not stimulate the release of IL-12, IL-23, IL-1 $\beta$ , IL-6 or TNF- $\alpha$  by DCs. This lack of toxicity is in line with the findings of Fisichella *et al.*<sup>49</sup> who showed that amine derivatized mesoporous silica microparticles elicit no toxic effect on cells and with the emerging opinion that the interaction of nanomaterials with the immune system necessitates careful assessment of nano-material toxicity.<sup>50</sup>

Similar results have been obtained upon DC treatment with carboxyl-micro-pSi (not shown). These results also demonstrate that micro-pSi suspensions are not contaminated by microorganisms or their derivatives capable of stimulating the immune cells.<sup>51</sup> For the purpose of exploiting the intrinsic luminescence of these microparticles, DCs were incubated with 0.5 mg mL<sup>-1</sup> of carboxyl- or amine-micro-pSi. The particles were ingested by the cells by an endocytosis mechanism as reported by Serda *et al.* for discoidal micro-pSi.<sup>52</sup> After 24 hours, the particle cellular uptake was visualized by confocal microscopy using different excitation wavelengths and detection channels. Fig. 6

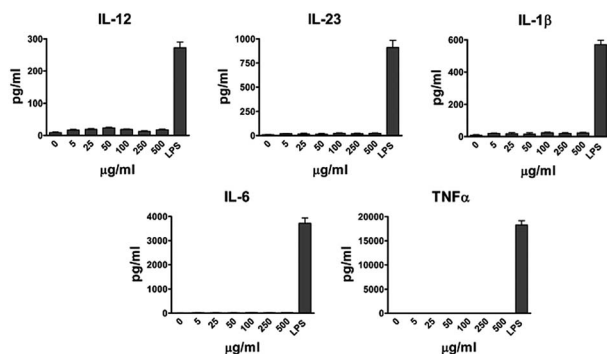


Fig. 5 Analysis of cytokine production by DCs treated for 24 hours with different doses of amine-micro-pSi or LPS used as the positive control. The results are the mean  $\pm$  SD of three experiments.

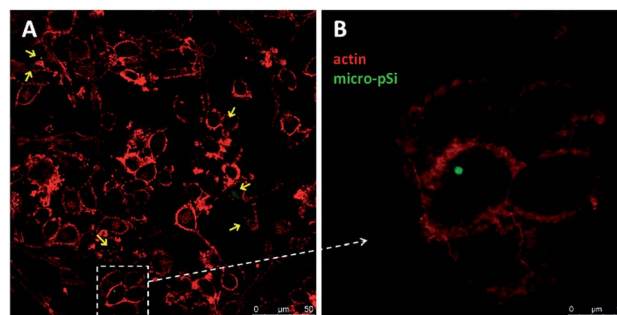


Fig. 6 Confocal microscopy images of DCs treated with 500  $\mu$ g of amino-micro-pSi (in green). After 24 hour incubation the cells were fixed and stained with Phalloidin to label filamentous F-actin (red). One representative experiment of three is shown. (A) Internal z-stack of a general field and (B) a zoom-in of (A).

(panel A) shows a confocal image from which it appears that amine-micro-pSi are efficiently internalized by human DCs and preserve a bright emission in the red region. The panel B is the zoom-in of the panel A field area enclosed in dashed lines, highlighting a cell showing an ingested particle. Similar results have been obtained using carboxyl-micro-pSi (results not shown), indicating that the presence of amine or carboxyl functionalities on the pSi surface did not change the particle uptake by DCs. In average 1.5 micro-pSi per cell were observed, corresponding to an ingested pSi volume of about 0.3  $\mu$ m<sup>3</sup> (0.05  $\mu$ m<sup>3</sup> of silicon).

Fig. 7 shows the excitation at 405 nm, which corresponds to the highest photon energy usually available for conventional

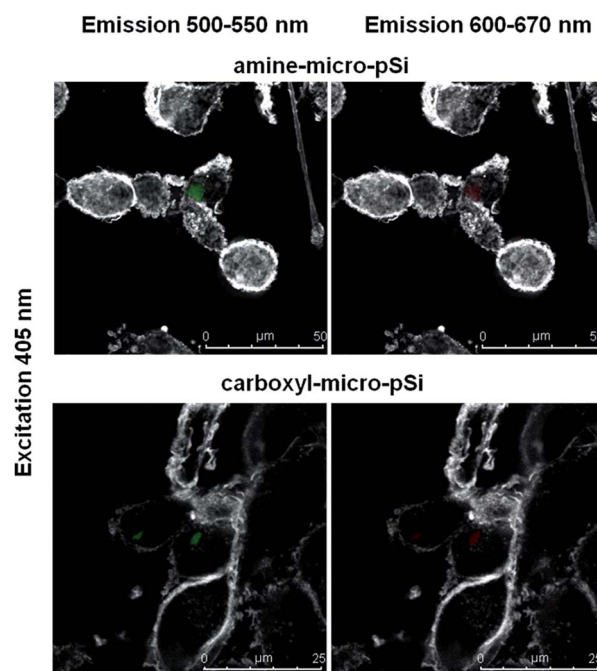


Fig. 7 Confocal microscopy analysis of amine- and carboxyl-micro-pSi ingested by DCs. The excitation is set at 405 nm and the emission collected in the green (left panel) and red (right panel) region.

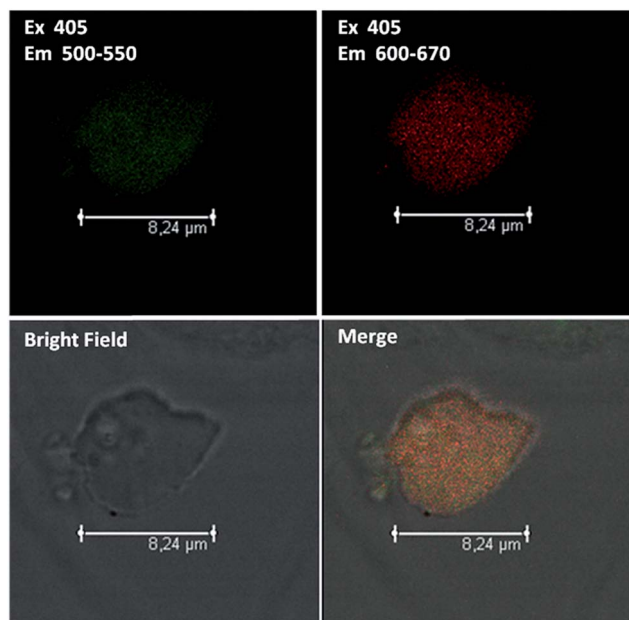


Fig. 8 Confocal microscopy images of an amine-micro-pSi. Excitation at 405 nm. Left top: emission collected in the range 500–550 nm; right top: emission collected in the range 600–650 nm; left bottom: bright field image; right bottom: merged image.

confocal microscopes, and acquiring the images with the red and green detection channels. This figure shows that the amine- and carboxyl-micro-pSi luminescence can be detected both at 500–550 nm (green) and 600–670 nm (red). In Fig. 8 we show the image of a single amino-micro-pSi particle obtained by excitation at 405 nm and acquisition in the green and red regions. The merged image is shown in the bottom right panel. The corresponding emission spectrum in the red region acquired by a single-particle detection set-up (excitation at 488 nm) is shown in Fig. 9. These data demonstrate that single amine-micro-pSi can be imaged and analysed both by a spectral or an imaging apparatus. Moreover, the broad PL of these microparticles provides a signal traceable by both green and red channels. This

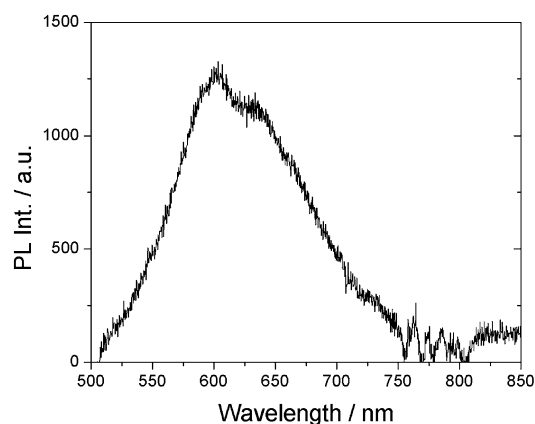


Fig. 9 PL emission from an amine-micro-pSi particle. Excitation at 488 nm.

property can help the intracellular localization of the micro-pSi or the tracking of the labelled cell, since the spectral region of detection can be chosen to be the one with lower interference from other fluorescence signals or from the background.

## 4 Conclusions

We were able to set-up a simple and well-assessed fabrication procedure and a functionalization protocol to obtain positively or negatively charged organic coating on micro-pSi. Fluorescence spectra show that the bright PL characteristic of native pSi is retained after functionalization. In addition to the pSi orange emission band (centred in the range 590–610 nm) related to quantum confinement, after introducing the amino groups a second emission band in the blue region (at about 420 nm) appears. This emission shows a different excitation pathway (confirmed by the lifetime range) and seems to be related to surface defect states introduced by the reaction with the diamine. We demonstrated that the micro-pSi particles are uptaken by primary human DCs and this process is not associated with a decrease in cell viability, even when the cells are incubated with very high concentrations of both amine- or carboxyl-micro-pSi. Furthermore, we did not observe any stimulation of the secretion of pro-inflammatory cytokines by DCs, suggesting that the particles do not activate these immune cells. The organic coating layer introduced by functionalization allows the microparticles to be effectively swallowed by DCs, indicating that these particles are good candidates as delivery vehicles to the immune cell system of drugs and anticancer vaccines. Finally, we clearly demonstrated by confocal microscopy that the optical properties of the micro-pSi studied here can be used to monitor the intracellular localization of the particles. This paper contributes significantly to the understanding and the successful exploitation of different emission mechanisms of pSi to perform a bio-medical experiment with a standard confocal microscope. The highly porous structure, in conjunction to the optical features and the absence of toxic effects, proposes these silicon microparticles as superior delivery vehicles traceable by conventional optical microscopes in cell cultures or in the tissue surface. A further improvement will be the use of the emerging multiphoton near-infrared microscopy techniques<sup>53,54</sup> which are expected to allow the microparticle localization at deeper (up to 500 μm) imaging depth.

## Acknowledgements

This work was done within the Nanomedicine Initiative funded by Fondazione Cariverona (Verona). The Nanoscience Laboratory of Trento was supported by Fondazione Caritro (Trento) and by the Italian Ministry of University and Research through the “Futuro in Ricerca” project RBFR12001G – NEMATIC. Marina Scarpa thanks Prof. Antonella Motta and Lorenzo Moschini, Department of Material Engineering, University of Trento, for the acquisition of SEM images.

## Notes and references

- 1 E. J. Anglin, L. Cheng, W. R. Freeman and M. J. Sailor, *Adv. Drug Delivery Rev.*, 2008, **60**, 1266.
- 2 R. E. Serda, B. Godin, E. Blanco, C. Chaippini and M. Ferrari, *Biochim. Biophys. Acta*, 2011, **1810**, 317.
- 3 J. Salonen, A. M. Kaukonen, J. Hirvonen and P. V. Lehto, *J. Pharm. Sci.*, 2008, **97**, 632.
- 4 F. Peng, Y. Su, Y. Zhong, C. Fan, S.-T. Lee and Y. He, *Acc. Chem. Res.*, 2014, **47**, 612.
- 5 C. A. Prestidge, T. J. Barnes, C.-H. Lau, C. Barnett, A. Loni and L. Canham, *Expert Opin. Drug Delivery*, 2007, **4**, 101.
- 6 L. T. Canham, *Adv. Mater.*, 1995, **7**, 1033.
- 7 D. M. Reffitt, R. Jogdaohsingh, R. P. Thompson and J. J. Powell, *J. Inorg. Biochem.*, 1999, **76**, 141.
- 8 G. Ledoux, O. Guillois, D. Porterat and C. Reynaud, *Phys. Rev. B: Condens. Matter Mater. Phys.*, 2000, **62**, 15942.
- 9 C. Delerue, G. Allan and M. Lannoo, *Phys. Rev. B: Condens. Matter Mater. Phys.*, 1993, **48**, 11024.
- 10 J. L. Gole, F. P. Dudel, D. Grantier and D. A. Dixon, *Phys. Rev. B: Condens. Matter Mater. Phys.*, 1997, **56**, 2137.
- 11 L. Gu, D. J. Hall, Z. Qin, E. J. Anglin Joo, D. J. Mooney, S. B. Howell and M. J. Sailor, *Nat. Commun.*, 2013, **4**, 2326.
- 12 D. S. English, L. E. Pell, Z. Yu, P. F. Barbara and B. A. Korgel, *Nano Lett.*, 2002, **2**, 681.
- 13 A. Saar, *J. Nanophotonics*, 2009, **3**, 032501.
- 14 M.-A. Shahbazi, M. Hamidi, E. M. Mäkilä, H. Zhang, P. V. Almeida, M. Kaasalainen, J. J. Salonen, J. T. Hirvonen and H. A. Santos, *Biomaterials*, 2013, **34**, 7776.
- 15 E. Tasciotti, X. Liu, R. Bhavane, K. Plant, A. D. Leonard, B. K. Price, M. M.-C. Cheng, P. Decuzzi, J. M. Tour, F. Robertson and M. Ferrari, *Nat. Nanotechnol.*, 2008, **3**, 151.
- 16 L. M. Bimbo, M. Sarparanta, H. A. Santos, A. J. Airaksinen, E. Mäkilä, T. Laaksonen, L. Peltonen, V.-P. Lehto, J. Hirvonen and J. Salonen, *ACS Nano*, 2010, **4**, 3023.
- 17 P. Decuzzi, B. Godin, T. Tanaka, S.-Y. Lee, C. Chiappini, X. Liu and M. Ferrari, *J. Controlled Release*, 2010, **141**, 320.
- 18 J. Rytönen, R. Miettinen, M. Kaasalainen, V.-P. Lehto, J. Salonen and A. Närvänen, *J. Nanomater.*, 2012, 896562, DOI: 10.1155/2012/896562.
- 19 B. Godin, J. Gu, R. E. Serda, R. Bhavane, E. Tasciotti, C. Chiappini, X. Liu, T. Tanaka, P. Decuzzi and M. Ferrari, *J. Biomed. Mater. Res., Part A*, 2010, **94**, 1236.
- 20 W. D. Kirkey, Y. Sahoo, X. G. Li, Y. Q. He, M. T. Swihart, A. N. Cartwright, S. Bruckenstein and P. N. Prasad, *J. Mater. Chem.*, 2005, **15**, 2028.
- 21 L. Gu, J.-H. Park, K. H. Duong, E. Ruoslahti and M. J. Sailor, *Small*, 2010, **6**, 2546.
- 22 W. Xu, J. Riikonen, T. Nissinen, M. Suvanto, K. Rilla, B. Li, Q. Wang, F. Deng and V.-P. Lehto, *J. Phys. Chem. C*, 2012, **116**, 22307.
- 23 B. Sweryda-Krawiec, R. R. Chandler-Henderson, J. L. Coffey, Y. G. Rho and R. F. Pinizzotto, *J. Phys. Chem.*, 1996, **100**, 13776.
- 24 R. R. Chandler-Henderson, B. Sweryda-Krawiec and J. L. Coffey, *J. Phys. Chem.*, 1995, **99**, 8851.
- 25 A. Verma and F. Stellacci, *Small*, 2010, **6**, 12.
- 26 C. Chang, *J. Autoimmun.*, 2010, **34**, J234.
- 27 M. Di Gioacchino, C. Tetrarca, F. Lazzarin, L. Di Giampaolo, E. Sabbioni, P. Boscolo, R. Mariani-Costantini and G. Bernardini, *Int. J. Immunopathol. Pharmacol.*, 2011, **24**(suppl. 1), 65S.
- 28 K. Schäkel, *Exp. Dermatol.*, 2009, **18**, 264.
- 29 F. Granucci, I. Zanoni and P. Ricciardi-Castagnoli, *Cell. Mol. Life Sci.*, 2008, **65**, 1683.
- 30 L. E. Paulis, S. Mandal, M. Kreutz and C. G. Figdor, *Curr. Opin. Immunol.*, 2013, **25**, 389.
- 31 M. P. Stewart and J. M. Buriak, *J. Am. Chem. Soc.*, 2001, **123**, 7821.
- 32 S. Kalkhof and A. Sinz, *Anal. Bioanal. Chem.*, 2008, **392**, 305.
- 33 J. Schindelin, I. Arganda-Carreras, E. Frise, V. Kaynig, M. Longair, T. Pietzsch, S. Preibisch, C. Rueden, S. Saalfeld, B. Schmid, J.-Y. Tinevez, D. J. White, V. Hartenstein, K. Eliceiri, P. Tomancak and A. Cardona, *Nat. Methods*, 2012, **9**, 676.
- 34 R. Herino, G. Bomchil, K. Barla, C. Bertrand and J. L. Ginoux, *J. Electrochem. Soc.*, 1987, **134**, 1994.
- 35 A. Halimaoui, in *Properties of porous silicon*, ed. L. T. Canham, INSPEC The Institution of Electrical Engineers, London, 1997, pp. 12–22.
- 36 O. Akbulut, C. R. Mace, R. V. Martinez, A. A. Kumar, Z. Nie, M. R. Patton and G. M. Whitesides, *Nano Lett.*, 2012, **12**, 4060.
- 37 Z. Qin, J. Joo, L. Gu and M. J. Sailor, *Part. Part. Syst. Charact.*, 2014, **31**, 252.
- 38 G.-B. Li, L.-S. Liao, X.-B. Liu, X.-Y. Hou and X. Wang, *Appl. Phys. Lett.*, 1997, **70**, 1284.
- 39 E. Froner, R. Adamo, Z. Gaburro, B. Margesin, L. Pavesi, A. Rigo and M. Scarpa, *J. Nanopart. Res.*, 2006, **8**, 1071.
- 40 A. Halimaoui, C. Oules, G. Bomchil, A. Bsiesy, F. Gaspard, R. Herino, M. Ligeon and F. Muller, *Appl. Phys. Lett.*, 1991, **59**, 304.
- 41 J. Fuzell, A. Thibert, T. M. Atkins, M. Dasog, E. Busby, J. G. C. Veinot, S. M. Kauzlarich and D. S. Larsen, *J. Phys. Chem. Lett.*, 2013, **4**, 3806.
- 42 L. Pavesi and M. Ceschini, *Phys. Rev. B: Condens. Matter Mater. Phys.*, 1993, **48**, 95781.
- 43 Y. Chao in *Comprehensive Nanoscience and Technology*, ed. D. L. Andrews, G. D. Scholes and G. P. Wiederrecht, Academic Press, Oxford, 2011, vol. 1, pp. 543–570.
- 44 M. Dasog, Z. Yang, S. Regli, T. M. Atkins, A. Faramus, M. P. Singh, E. Muthuswamy, S. M. Kauzlarich, R. D. Tilley and J. G. C. Veinot, *ACS Nano*, 2013, **7**, 2676.
- 45 D. A. Vignali and V. K. Kuchroo, *Nat. Immunol.*, 2012, **13**, 722.
- 46 M. Xu, I. Mizoguchi, N. Morishima, Y. Chiba, J. Mizoguchi and T. Yoshimoto, *Clin. Dev. Immunol.*, 2010, **2010**, 832454.
- 47 J. K. Elmquist, T. E. Scammell and C. B. Saper, *Trends Neurosci.*, 1997, **20**, 565.
- 48 A. F. Suffredini, G. Fantuzzi, R. Badolato, J. J. Oppenheim and N. P. O'Grady, *J. Clin. Immunol.*, 1999, **19**, 203.
- 49 M. Fisichella, H. Dabboue, S. Bhattacharyya, M. L. Saboungi, J. P. Salvétat, T. Hervor and M. Guerin, *Toxicol. In Vitro*, 2009, **23**, 697.

- 50 B. Fadeel, *Swiss Med. Wkly.*, 2012, **142**, w13609.
- 51 B. Fadeel and A. E. Garcia-Bennett, *Adv. Drug Delivery Rev.*, 2010, **62**, 362.
- 52 R. E. Serda, S. Ferrati, B. Godin, E. Tasciotti, X. W. Xu and M. Ferrari, *Nanoscale*, 2009, **1**, 250.
- 53 J.-H. Park, L. Gu, G. von Maltzahn, E. Ruoslahti, S. N. Bhatia and M. J. Sailor, *Nat. Mater.*, 2009, **8**, 331.
- 54 P. Sarder, S. Yazdanfar, W. J. Akers, R. Tang, G. P. Sudlow, C. Egbulefu and S. Achilefu, *J. Biomed. Opt.*, 2013, **18**, 106012.